

ARTICLE



Deficiency of thiosulfate sulfurtransferase mediates the dysfunction of renal tubular mitochondrial fatty acid oxidation in diabetic kidney disease

Jia Xiu Zhang ¹, Pei Pei Chen^{1,2}, Xue Qi Li ¹, Liang Li¹, Qin Yi Wu¹, Gui Hua Wang¹, Xiong Zhong Ruan ³ and Kun Ling Ma^{1,2}✉

© The Author(s), under exclusive licence to ADMC Associazione Differenziamento e Morte Cellulare 2024

One of the main characteristics of diabetic kidney disease (DKD) is abnormal renal tubular fatty acid metabolism, especially defective fatty acid oxidation (FAO), accelerating tubular injury and tubulointerstitial fibrosis. Thiosulfate sulfurtransferase (TST), a mitochondrial enzyme essential for sulfur transfer, is reduced in metabolic diseases like diabetes and obesity. However, the potential role of TST in regulating fatty acid metabolic abnormalities in DKD remains unclear. Here, our data revealed decreased TST expression in the renal cortex of DKD patients. TST deficiency exacerbated tubular impairment in both diabetic and renal fibrosis mouse models, while sodium thiosulfate treatment or TST overexpression mitigated renal tubular injury with high-glucose exposure. TST downregulation mediated the decrease in S-sulfhydration of very long-chain specific acyl-CoA dehydrogenase, resulting in mitochondrial FAO dysfunction. This sequence of events exacerbates the progression of tubulointerstitial injury in DKD. Together, our findings demonstrate TST as a regulator of renal tubular injury in DKD.

Cell Death & Differentiation; <https://doi.org/10.1038/s41418-024-01365-8>

INTRODUCTION

Diabetic kidney disease (DKD) is a long-term microvascular complication of diabetes mellitus, characterized by glucose-induced renal injury in conjunction with inflammation [1], fibrosis [2], and compromised mitochondrial metabolic adaptability [3]. The progression of DKD is notably impacted by renal interstitial fibrosis, predominantly characterized by the abnormal expression of profibrotic factors [4], the activation of myofibroblasts [5], and the occurrence of epithelial-to-mesenchymal transition [6]. Under physiological conditions, renal tubular epithelial cells favor long-chain fatty acids as the primary energy substrate through mitochondrial fatty acid oxidation (FAO). A burgeoning body of evidence suggests that disrupted FAO contributes to renal fibrosis in the context of chronic kidney diseases [7–9], with the restoration of FAO, either genetically or pharmaceutically, potentially improving renal fibrosis [10–12].

The FAO pathway encompasses a range of oxidation processes, with mitochondrial β -oxidation serving as the principal mechanism for metabolizing long-chain fatty acids [13]. An acyl-CoA dehydrogenase facilitates the initial conversion of acyl-CoA into trans-2-enoyl-CoA in the mitochondrial β -oxidation pathway. Notably, the very long-chain acyl-CoA dehydrogenase (VLCAD) catalyzes the dehydrogenation of acyl-CoA, accommodating carbon chains from 12 to 24 units long. Some studies have shown that deficiency of the VLCAD caused disorders in mitochondrial FAO of long-chain fatty acids, potentially leading to complications such as hypoglycemia, rhabdomyolysis,

cardiomyopathy, hepatic insufficiency, and even sudden death [14]. The enhanced catalytic efficiency of VLCAD, driven by an S-nitrosylation at Cys238, has been observed to regulate mitochondrial FAO in the liver of ob/ob mice [15]. In addition, VLCAD has been identified as a critical factor for mitochondrial metabolism in leukemia cells [16]. However, the effect of VLCAD on diabetic renal tubular injury remains to be elucidated.

Thiosulfate sulfurtransferase (TST), commonly known as rhodanese, is an abundantly expressed mitochondrial enzyme that plays a pivotal role in sulfur metabolism [17]. It was originally recognized for its involvement in cyanide detoxification, a process facilitated by TST through the use of sodium thiosulfate (STS) as a sulfur donor for cyanide sulfonation. Interestingly, a previous study revealed an inverse relationship between TST activity and the incidence of obesity and insulin resistance [18]. A recent study found an upregulated hepatic expression of carnitine palmitoyltransferase 1 α in transgenic mice with adipocyte-specific overexpression of TST, implying an enhanced capacity for hepatic mitochondrial FAO. Carter et al. found medium-chain FAO was defective and mitochondrial respiration was increased in the hepatocytes of TST knockout (KO) mice [19].

S-sulfhydration, or persulfidation [20], a post-translational protein modification that involves the attachment of a hydro-persulfide molecule to a cysteine residue of a target protein, has only recently come to light. Mass spectrometry data suggest that the livers of TST KO mice possess reduced levels of S-sulfhydrated proteins pivotal to lipid oxidation pathways [19]. Importantly, thiosulfate exposure reactivates the complex I subunit NADH

¹Institute of Nephrology, Zhong da Hospital, School of Medicine, Southeast University, Nanjing, China. ²Department of Nephrology, The Second Affiliated Hospital, School of Medicine, Zhejiang University, Hangzhou, China. ³Centre for Lipid Research, Key Laboratory of Molecular Biology on Infectious Diseases, Ministry of Education, Chongqing Medical University, Chongqing, China. ✉email: klma@zju.edu.cn

Received: 10 February 2024 Revised: 11 August 2024 Accepted: 14 August 2024

Published online: 22 August 2024

dehydrogenase previously inhibited, when mediated by bovine rhodanese [21]. Nevertheless, it is still undetermined how TST affects renal function and S-sulfhydrated kidney proteins in DKD.

Therefore, this study aims to elucidate whether dysregulation of TST expression might modulate the S-sulfhydration of VLCAD, thereby potentially instigating mitochondrial FAO dysfunction in renal tubular epithelial cells and possibly exacerbating the progression of tubulointerstitial injury in DKD.

RESULTS

TST expression was decreased in renal tubular epithelial cells of patients with DKD or in HK-2 cells exposed to high glucose

We examined TST expression in renal biopsy samples obtained from 16 individuals with DKD and 12 individuals who underwent nephrectomy without DKD but with renal cell carcinoma (Supplementary Tables 1 and 2). The immunohistochemical (IHC) analysis demonstrated that TST was predominantly expressed in renal tubular epithelial cells (Fig. 1a). Most notably, TST expression was markedly reduced in the renal tubules of patients with DKD. This diminution in TST levels was inversely correlated with the area of extracellular matrix deposition, as indicated by fibronectin staining (Fig. 1b, c). In addition, we further confirmed that TST expression significantly decreased in human kidney-2 (HK-2) cells treated with high glucose (HG) (Fig. 1d–g).

Diabetic TST knockout mice worsened renal fibrosis

The functional implications of TST in the progression of DKD were investigated through hyperglycemia induction via streptozocin (STZ) in wild-type (WT) mice [22] and systemic TST KO mice. The results showed the absence of TST expression in the renal tissue of TST KO mice that confirmed the successful establishment of TST deficiency (Fig. 2a, b). Both diabetic WT mice and TST KO mice demonstrated elevated fasting blood glucose levels compared to non-diabetic WT mice (Supplementary Table 3). Interestingly, the urine albumin/creatinine ratio (ACR) of diabetic TST KO mice significantly exceeded that of diabetic WT mice, suggesting an aggravation of renal impairment due to TST deficiency (Fig. 2c). The renal epithelial injury marker, urinary Kim-1, was markedly higher in the TST KO + DM group compared to the DM group alone (Fig. 2d). Additionally, renal hypertrophy was evident in diabetic mice, as indicated by the kidney weight to body weight ratio (Fig. 2e). Histological examination of renal tissue revealed advanced tubular damage in diabetic TST KO mice, including cell swelling and vacuolization (Fig. 2f). Despite the slight tubulointerstitial fibrosis in STZ-induced model, the expression of α -SMA and fibronectin highlighted a more significant fibrotic development in diabetic TST KO kidneys compared to diabetic WT kidneys (Fig. 2g, h and Supplementary Fig. 1a). Mitochondrial morphological changes in cortical proximal tubules were assessed using transmission electron microscopy (TEM). A pronounced disruption of mitochondrial structure was seen in diabetic TST KO mice, manifesting as swollen and fragmental (Fig. 2i).

The effects of TST on renal fibrosis were carried out using the unilateral ureteral obstruction nephropathy (UUO) kidney fibrosis model. Seven days post-surgery, TST KO mice presented with heightened tubular damage and interstitial fibrosis compared to WT mice, reinforcing the potential protective function of TST in renal tubulointerstitial fibrosis (Supplementary Fig. 2a–o). When comparing TST KO mice to WT controls, periodic acid-Schiff (PAS) staining showed that the degree of tubular atrophy and dilatation brought on by UUO was more severe (Supplementary Fig. 2a, b). Consistent with these findings, TEM images illustrated mitochondrial rupture and swelling in renal cortical proximal tubules post-UUO surgery (Supplementary Fig. 2p).

Overexpression of TST conferred protection against diabetic kidney fibrosis

To elucidate the role of TST in diabetic kidney damage, we conducted an experiment wherein mice were treated with adeno-

associated virus 9 (AAV9)-TST to enhance TST expression and AAV9-Control to act as a baseline comparator. Notably, the TST protein expression in the renal tubular cells was significantly heightened in diabetic mice treated with AAV9-TST compared to those treated with AAV9-Control (Supplementary Fig. 3a, b). This increased expression was concomitant with observed improvements in renal tubular injury and renal fibrosis (Supplementary Fig. 3c–m). PAS staining showed that TST overexpression could significantly improve the atrophy and necrosis of renal tubular epithelial cells induced by diabetes (Supplementary Fig. 3f). Compared to the swollen and spherical mitochondria in diabetic mice, TST overexpression in renal epithelial cells corrected the majority of observed mitochondrial morphological alterations (Supplementary Fig. 3n).

Thiosulfate treatment protected kidneys from diabetic lesions via TST activation

TST has been identified as a rhodanese to cyanide detoxification, where the therapeutic antidote thiosulfate operates as a TST substrate facilitating the sulfane-sulfur transfer reaction [23]. Our study showed a notable augmentation in TST expression due to STS administration in the diabetic cohort (Fig. 3a, b). Furthermore, STS intervention reduced the severity of diabetic renal tubular injury throughout the 12-week experimental timeline (Fig. 3c–f). Additionally, PAS staining demonstrated that STS treatment ameliorated tubular injuries in diabetic mice, which were characterized by edema and tubular brush loss (Fig. 3f). Diabetic kidneys receiving STS exhibited markedly lessened expressions of renal fibrosis proteins (Fig. 3g, h and Supplementary Fig. 1b), alongside morphological modification of mitochondria as illustrated by TEM (Fig. 3i). Alanine transaminase and aspartate transaminase activities were lower in STS-treated diabetic mice, demonstrating STS's biosafety (Fig. 3j). Cell viability was not adversely affected across varying STS concentrations (Fig. 3k, l).

TST overexpression ameliorated the injury of renal tubular epithelial cells caused by high glucose

Our further exploration into TST's effects on renal tubular epithelial cells involved the upregulation of TST expression via TST plasmid transfection into HK-2 cells and primary tubular epithelial cells (PTEC), followed by HG exposure. TST overexpression resulted in reduced expression of profibrotic markers in HK-2 cells and PTEC subjected to HG conditions (Fig. 4a and Supplementary Fig. 4a). Despite a lack of substantial changes in mitochondrial membrane potential (MMP), reactive oxygen species (ROS) production was diminished and adenosine triphosphate (ATP) levels were amplified following TST overexpression in HK-2 cells (Fig. 4b–d). Overexpression of TST overrode the change of mitochondrial morphology, which was shown by improved mitochondrial aspect ratio and form factor in HG-induced HK-2 cells (Fig. 4e, f). To discern the metabolic pattern shift, we evaluated the oxygen consumption rate (OCR) of HK-2 cells and PTEC with TST overexpression in HG or normal glucose (NG) media. Results showed that HG exposure reduced ATP generation, maximal respiration, spare respiratory capacity, and basal respiration, whereas TST overexpression significantly enhanced these indices, indicating a successful resuscitation of mitochondrial respiration (Fig. 4g and Supplementary Fig. 4b). A decline in ATP generation, spare respiratory capacity and maximum respiration was evident in PTEC from TST KO mice when exposed to HG, compared to WT counterparts (Supplementary Fig. 4c).

STS treatment alleviated HG-induced tubular epithelial cell dysfunction and mitochondrial damage

Treatment with STS mitigated the high expression of renal profibrotic markers instigated by HG in renal tubular cell (Fig. 5a

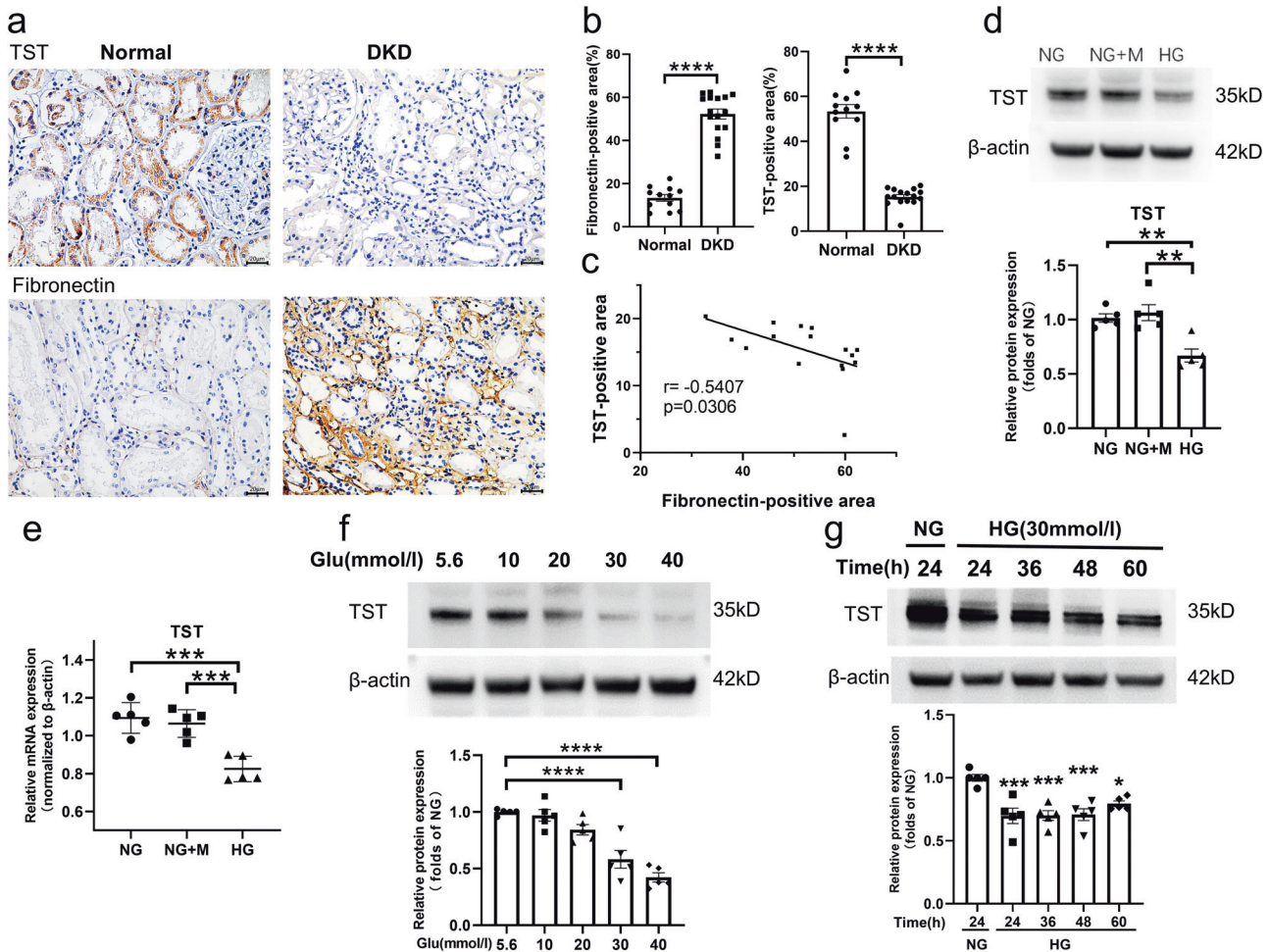


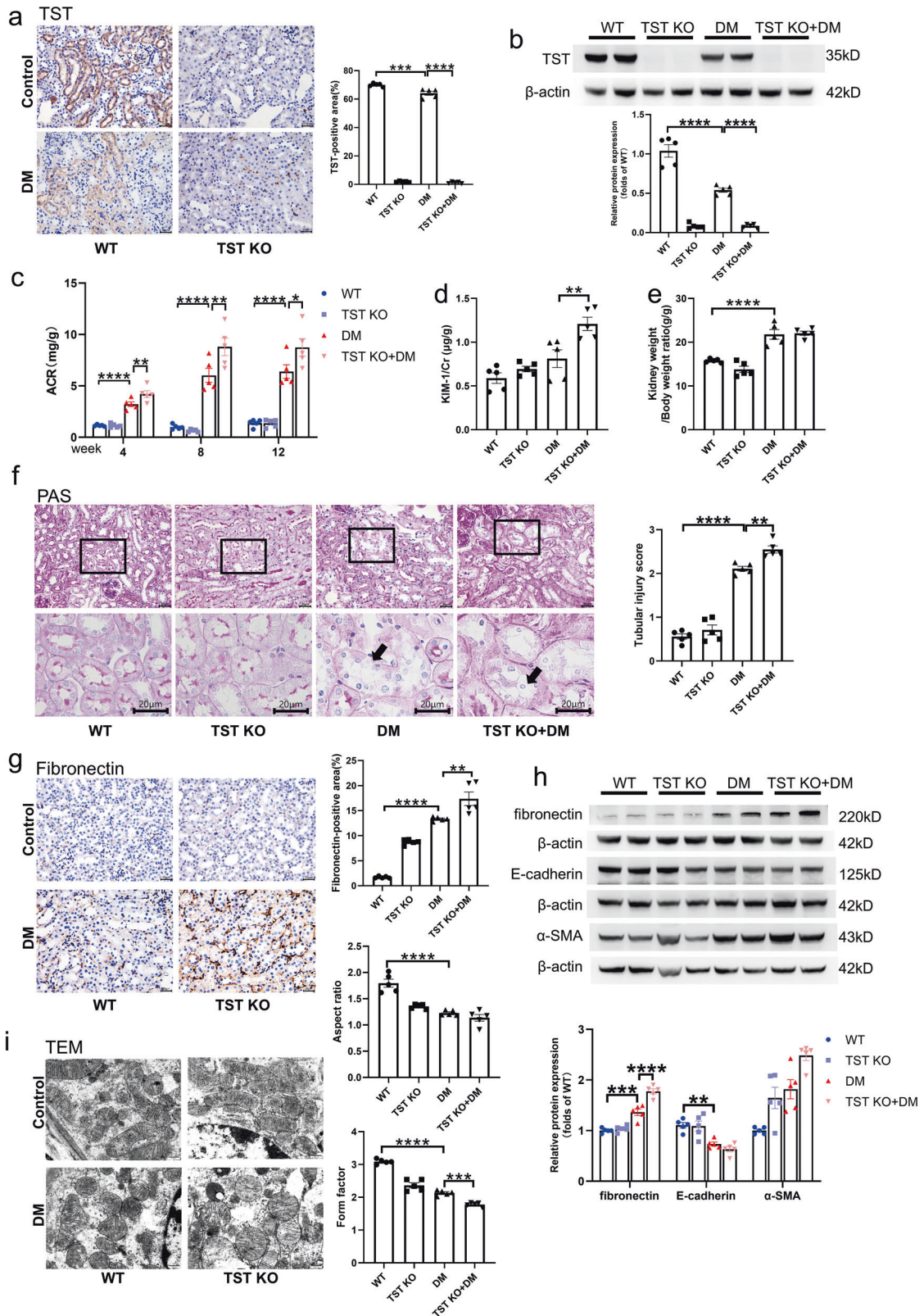
Fig. 1 TST expression was decreased in renal tubular epithelial cells of patients with DKD or in HK-2 cells exposed to high glucose. **a, b** Representative images from IHC and quantification of tubular TST and fibronectin expression in human renal cortical tissues from normal individuals ($n = 12$) or DKD patients ($n = 16$) (Original magnification $\times 400$, Scale bars, $20 \mu\text{m}$). **c** Correlation between TST expression and fibronectin in patients with DKD. **d** Representative western blot images and summarized data showing relative protein levels of TST in HK-2 cells treated with NG (normal glucose, 5.6 mmol/l), HG (high glucose, 30 mmol/l) or NG + M (normal glucose + D-mannitol, 24.4 mmol/l) for 48 h ($n = 5$). β -actin was used as an internal control and the levels of protein expression normalized to the NG group. **e** Real-time PCR analysis of TST mRNA levels in HK-2 cells treated with NG, HG, or NG + M for 48 h ($n = 5$). **f** Representative western blot images and summarized data showing relative protein levels of TST in HK-2 cells treated with different glucose concentrations ($5.6, 10, 20, 30, 40 \text{ mmol/l}$) for 48 h ($n = 5$). **g** Representative western blot images and summarized data showing relative protein levels of TST in HK-2 cells treated with NG or HG for varying durations ($24, 36, 48, 60 \text{ h}$). $**P < 0.01$; $***P < 0.001$ vs. NG, ($n = 5$ for each group). Data are expressed as mean \pm SEM. $*P < 0.05$, $**P < 0.01$, $***P < 0.001$, $****P < 0.0001$. Unpaired Student's *t*-test (**b**), one-way ANOVA (**d-g**).

and Supplementary Fig. 4d). HG exposure caused a decrease in both ATP levels and MMP within renal tubular cells, a trend in which STS treatment effectively reversed (Fig. 5b, d). The administration of STS was further associated with a marked reduction in ROS production when compared to the HG group (Fig. 5c). Notably, the mitochondrial morphology was recovered, and the mitochondrial shape transitioned from short and round to elongated and flat in the STS-treated HG group, as opposed to the HG group (Fig. 5e, f). Findings from the OCR suggested that STS treatment facilitated an enhancement in renal tubule mitochondrial activity (Fig. 5g and Supplementary Fig. 4e).

TST maintained mitochondrial FAO homeostasis in renal tubular epithelial cells in diabetic conditions

The crucial role of metabolic alterations in renal tubular cells in DKD is well-documented [24]. TST shows to be a significant player in metabolic disease [17]. Consequently, we employed targeted metabolomics of the renal cortex to elucidate the metabolic pathways influenced by TST deficiency. Pronounced metabolic

differences among the four groups of mice were observed (Supplementary Fig. 5a). The apparent differential metabolites were mainly clustered in acylcarnitines, nucleic acid metabolites, and organic acids (Fig. 6a). Both DKD and chronic kidney disease share a characteristic accumulation of long-chain acylcarnitines in renal tissues, indicative of an aberration in mitochondrial fatty acid β -oxidation [25, 26]. Notably, our study showed that the kidneys of diabetic TST KO mice compared to diabetic WT mice displayed heightened levels of long-chain acylcarnitines (Fig. 6b), whereas a decrease in long-chain acylcarnitines was detected in the diabetic group treated with STS relative to diabetic control mice (Fig. 6c). These findings point toward a potential link between mitochondrial fatty acid β -oxidation dysregulation and TST expression. Changes in medium-chain and short-chain acylcarnitines in the renal cortex were not consistent and evident in diabetic TST KO mice or diabetic animals treated with STS as compared to normal diabetic mice (Supplementary Fig. 5b–e). To further investigate the role of TST in FAO, we overexpressed TST with a TST plasmid in PTEC prior to HG stimulation in vitro. Our observations showed



that TST upregulation significantly enhanced FAO activity, manifested by notable shifts in maximal respiration in the presence or absence of the carnitine palmitoyltransferase 1 inhibitor, etomoxir (Eto), relative to the HG group (Fig. 6d, e). STS treatment increased the FAO capacity of renal tubules,

thereby effectively ameliorating the metabolic dysregulation induced by HG levels (Fig. 6f and Supplementary Fig. 5f). We performed stable isotope tracing tests using a uniformly labeled ¹³C₁₆ palmitate tracer in PTEC to further explore the impact of TST on long-chain FAO. In PTEC exposed to HG levels, we observed

Fig. 2 Diabetic TST knockout mice worsened renal fibrosis. Male WT and TST KO mice were administered with STZ or citrate buffer. **a** Representative immunohistochemical staining images and quantification illustrating expressions of TST in the kidneys from WT, TST KO, diabetic WT, and diabetic TST KO groups ($n = 5$) (Original magnification $\times 400$, Scale bars, $20 \mu\text{m}$). **b** Representative western blot images and summarized data showing relative protein levels of TST in the kidneys from WT, TST KO, diabetic WT, and diabetic TST KO groups ($n = 5$). **c** ACR evaluated at 4, 8, and 12 weeks post-initial STZ injection ($n = 5$). **d, e** Urinary Kim-1/creatinine ratio and kidney-to-body weight ratio in the WT, TST KO, diabetic WT, and diabetic TST KO groups ($n = 5$). **f** PAS-stained photomicrographs displaying tubular structural changes in the WT, TST KO, diabetic WT, and diabetic TST KO groups. Arrows indicate renal tubular injury. (Original magnification $\times 400$, Scale bars, $20 \mu\text{m}$). **g** Representative immunohistochemical staining images and quantification illustrating expressions of fibronectin in the kidneys from WT, TST KO, diabetic, and diabetic TST KO groups ($n = 5$) (Original magnification $\times 400$, Scale bars, $20 \mu\text{m}$). **h** Representative western blot images and summarized data showing relative protein levels of fibronectin, α -SMA, and E-cadherin in the kidneys from WT, TST KO, diabetic WT, and diabetic TST KO groups ($n = 5$). **i** Representative photomicrographs and quantification of renal tubular mitochondrial morphological changes by transmission electron microscopy (TEM) analysis ($n = 5$) (Original magnification $\times 8000$, Scale bars, 500nm). Data are expressed as mean \pm SEM. * $P < 0.05$, ** $P < 0.01$, *** $P < 0.001$, **** $P < 0.0001$. One-way ANOVA (**a–i**, except for α -SMA expression in (**h**)) or Kruskal–Wallis test (α -SMA expression in (**h**)).

significant reductions in medium and short-chain acylcarnitines generated from the $^{13}\text{C}_{16}$ palmitate, further indicating long-chain FAO inhibition (Supplementary Fig. 5g, h). The end product of the FAO pathway, $^{13}\text{C}_2$ acetyl-carnitine, increased in HG-treated PTEC upon treatment with TST overexpression or STS, indicating an improvement in long-chain FAO dysfunction (Fig. 6g, h).

TST promoted S-sulfhydration of VLCAD

TST deficiency has been associated with low hepatic protein persulfidation, which includes a reduction in the S-sulfhydration of the acyl-CoA dehydrogenase family [19]. In this context, we examined the influence of TST on VLCAD S-sulfhydration, particularly with respect to alterations in the metabolism of long-chain fatty acids. The biotin–thiol labeling assay revealed that diabetic TST KO exhibited decreasing renal DTT-sensitive S-sulfhydration of VLCAD (Fig. 7a). The same pattern was evident in the kidneys of UJO model mice, underscoring the global role of TST in modulating VLCAD S-sulfhydration (Supplementary Fig. 2q). Conversely, overexpression of TST increased S-sulfhydrated VLCAD in the renal cortex of diabetic mice (Supplementary Fig. 3o). Comparable results were documented in HK-2 cells transfected with pl-TST and challenged by HG levels in vitro (Fig. 7b). When treated with STS, there was a pronounced increase in S-sulfhydrated VLCAD in both diabetic mice and HG-induced cells (Fig. 7c, d).

VLCAD features four evolutionarily conserved cysteine residues located within the catalytic region (Supplementary Table 8). To ascertain the cysteine target, we generated a sequence of mutants by substituting Cys215, Cys237, Cys433, and Cys477 with serine. Following transfection into HEK-293T cells, the S-sulfhydration level of the Cys237S mutant was found to be significantly less than that of the WT VLCAD and the other serine-substituted mutants (Fig. 7e). Similarly, in HK-2 cells, downregulation of VLCAD S-sulfhydration brought on by HG may be improved by overexpressing VLCAD but not C237S mutant (Fig. 7f).

VLCAD Cys237 is crucial to sustain mitochondrial FAO homeostasis in renal tubular epithelial cells under diabetic and high-glucose conditions

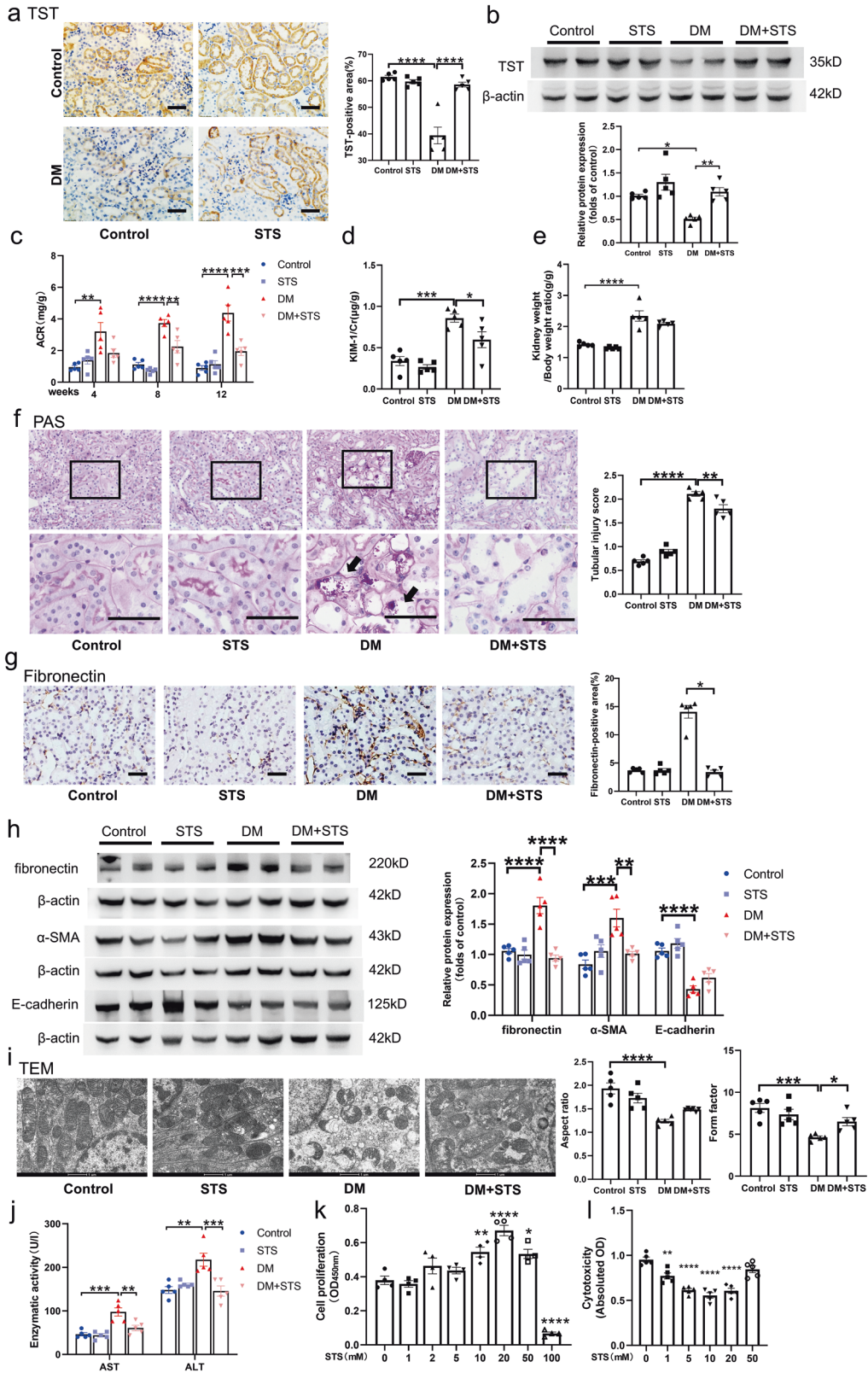
To elucidate the role of S-sulfhydrated VLCAD, we conducted transfection experiments with WT VLCAD, mutant Cys237S, and a blank control plasmid. Our findings indicate that VLCAD upregulation caused a decrease in ROS production and an enhancement of MMP in HK-2 cells under HG conditions, thereby demonstrating its protective effects on renal tubular mitochondria from HG-induced stress. In contrast, the Cys237S mutant was associated with amplified ROS production, diminished MMP, and reduced ATP levels when compared to the WT VLCAD under HG conditions (Supplementary Fig. 6a–c). Results from the OCR study revealed that, in contrast to the Cys237S mutant, VLCAD overexpression facilitated an improvement in renal tubule mitochondrial activity (Supplementary Fig. 6d). Further, our

assessment of FAO activity, gauged through the variance in maximal respiration levels with and without Eto, revealed that PTEC overexpressing the mutant Cys237S displayed a significant reduction in FAO activity when compared to those overexpressing WT VLCAD (Supplementary Fig. 6e). This underscored the pivotal role of VLCAD Cys237 in the preservation of mitochondrial FAO homeostasis. Our findings indicate that VLCAD overexpression effectively ameliorated HG-induced fibrotic state in HK-2 cells, whereas the Cys237S mutant did not exhibit these effects (Fig. 7g). This also suggests that the modulation of mitochondrial FAO through S-sulfhydration of VLCAD is instrumental in mitigating HG-induced renal tubular dysfunction.

DISCUSSION

The disruption in renal tubular lipid metabolism, particularly lipid accumulation [26] and FAO dysregulation, is one of the main characteristics of DKD. Fibrotic kidneys exhibit an accumulation of carnitine-conjugated long-chain fatty acids, indicative of deficiencies in mitochondrial fatty acid metabolism [25]. Studies conducted on diabetic patients have revealed elevated levels of plasma/serum acylcarnitines in DKD patients compared to diabetic counterparts without kidney disease [27], and these findings predicted DKD progression [28]. Sprague-Dawley rats with STZ-induced diabetes showed accumulation of acylcarnitine species in the combined renal cortex and the outer strip of the outer medulla within 2 weeks post-diabetes onset, signifying FAO dysregulation even at such an early stage [29]. Comparatively, db/db mice demonstrated accumulated long-chain acylcarnitines (C14 and C16) in the renal cortex at ages 12 and 24 weeks [27]. We found significant accumulation of long-chain acylcarnitine in the renal cortex of diabetic mice, suggesting that long-chain acylcarnitine accumulation may be a phenotype of early diabetic kidney injury. In addition, it was reported that hepatocyte respiration induced by octanoate was significantly reduced in TST KO mice compared to normal hepatocytes, suggesting impairment of medium-chain FAO due to TST KO [19]. In diabetic TST KO mice, we observed an intensified FAO disorder, as evidenced by increased accumulation of long-chain acylcarnitines. Taken together with in vitro results, we conclude that TST could regulate FAO to exert reno-protective effects.

STS has traditionally been employed in treating diseases such as cyanide poisoning [23], cisplatin-induced hearing loss [30], and calyphylaxis [31]. STS has also demonstrated protective effects in metabolic disorders. In experiments with db/db diabetic mice, STS administration effectively mitigated high fat diet-induced glucose intolerance and accompanying conditions such as polydipsia, polyuria, insulin resistance, and elevated levels of glycosylated hemoglobin [18]. Further, our findings indicate that STS could ameliorate FAO dysfunction in renal tubular epithelial cells, as suggested by reduced levels of renal long-chain acylcarnitine. Marutani et al. have shown [32], using the human neuroblastoma



cell line SH-SY5Y, that STS can decrease caspase-3 activity via increasing the S-sulfhydration of Cys163. We provide evidence that STS may potentially attenuate interstitial fibrosis in DKD by augmenting TST expression and enhancing S-sulfhydration of VLCAD in tubular cells.

During the process of S-sulfhydration, cysteine thiol groups (-SH) are converted to persulfide groups (-SSH), a post-translational modification that alters the activity of the modified protein, contingent on the acid dissociation constants of cysteine residues [33]. It is known that aging induces changes in the renal

Fig. 3 Thiosulfate treatment protected kidneys from diabetic lesions via TST activation. Male mice were injected with STZ or citrate buffer. Following successful diabetes induction, mice received daily oral doses of sodium thiosulfate (0.4 g/kg, STS). **a** Representative photomicrographs and quantification showing TST expression in the kidneys of normal control or diabetic mice with or without STS treatment ($n = 5$) (Original magnification $\times 400$, Scale bars, 20 μm). **b** Representative western blot images and summarized data shown with the relative protein levels of TST in the kidneys of normal control or diabetic mice with or without STS treatment ($n = 5$). **c** ACR measurement at 4, 8, and 12-week intervals post-initial STZ injection ($n = 5$). **d, e** Urinary Kim-1/creatinine ratio and kidney weight to body weight ratio in control or diabetic mice with or without STS treatment ($n = 5$). **f** Photomicrographs depict tubular structure alterations post-PAS staining. Arrows indicate renal tubular injury (Magnification $\times 400$, Scale bars, 50 μm). **g** Representative photomicrographs and quantification showing fibronectin expression in the kidneys of control or diabetic mice with or without STS treatment ($n = 5$) (Original magnification $\times 400$, Scale bars, 20 μm). **h** Representative western blot images and summarized data shown with the relative protein levels of fibronectin, α -SMA, and E-cadherin in the kidneys of control or diabetic mice with or without STS treatment ($n = 5$). **i** Representative photomicrographs and quantifications of renal tubular mitochondrial morphological changes via TEM analysis ($n = 5$) (Original magnification $\times 8000$, Scale bars, 500 nm). **j** Serum alanine aminotransferase (ALT) and aspartate aminotransferase (AST) activity measured in various mice groups using an automatic biochemistry analyzer ($n = 5$). **k, l** CCK8 assays ($n = 4$) and lactate dehydrogenase (LDH) cytotoxicity colorimetric assay ($n = 5$) in HK-2 cells after treatment with increased doses of STS. * $P < 0.05$, ** $P < 0.01$, *** $P < 0.001$, **** $P < 0.0001$ vs. the group without STS treatment. Data are expressed as mean \pm SEM. * $P < 0.05$, ** $P < 0.01$, *** $P < 0.001$, **** $P < 0.0001$. One-way ANOVA (**a–f, h–l** except for aspect ratio in **(i)**) or Kruskal–Wallis test (**g**, aspect ratio in **(i)**).

sulfhydryl, with most S-sulfhydrated proteins implicated in metabolic pathways. Notably, these proteins are typically localized within the mitochondrial matrix and the organelle lumen [34]. Furthermore, Sirtuin 3 has been shown to be S-sulfhydrated to enhance mitochondrial function and minimize oxidative damage in cisplatin-induced acute renal injury [35]. Polysulfide-mediated sulfhydration of Sirtuin1 has been shown to protect against diabetic nephropathy [36]. We posit that, for the first time, enhanced S-sulfhydration of VLCAD could potentially modify FAO dysfunction in renal tubular epithelial cells, serving as a proactive strategy against diabetic renal fibrosis.

VLCAD, a homodimer that resides within the inner mitochondrial membrane, is composed of subunits of 67 kDa each. Specific point mutations in the human variant of VLCAD are linked to a congenital metabolic disorder, which can manifest with severe pathophysiologic consequences such as cardiomyopathy, hypoglycemia, and rhabdomyolysis [37]. Our research revealed that VLCAD plays a crucial role in maintaining the health of renal tubular epithelial cells and their mitochondria. We also established that S-sulfhydration of Cys237 in human VLCAD markedly ameliorated FAO dysfunction, protecting renal tubular cells from HG.

There are some limitations in this study. We conducted in vivo experiments by using TST global KO mice and AAV9-mediated TST overexpression model. In comparison, renal tubule-specific TST overexpression could be a superior strategy. Another limitation is that we were unable to conduct the persulfidomic profiles of diabetic kidneys due to the restrictions of experimental technologies. Persulfidomic profiles could provide a more comprehensive picture of S-sulfhydrated proteins controlled by TST in renal tubular epithelial cells [38].

In summary, we have, for the first time, delineated the role of TST in mitigating diabetic renal tubular injury. Our findings illustrate that a decline in TST expression in renal tubular epithelial cells is associated with a decrease in S-sulfhydration of VLCAD, subsequently leading to mitochondrial FAO dysfunction and the exacerbation of tubulointerstitial injury in DKD. Our experiments also suggest that the administration of STS has potential therapeutic value in countering the progressive effects of DKD. These findings add to our understanding of TST's biological functions within the kidney and suggest that it plays a critical role in the onset and progression of tubulointerstitial fibrosis in DKD.

MATERIALS AND METHODS

Experimental animals

All in vivo procedures were carried out in accordance with protocols approved by the Animal Care and Use Committee of Southeast University, Nanjing, China (Approval No. 20210227025). Mice (3–5 mice/cage) housed in a standard, pathogen-free environment operating on a 12-h light/12-h

dark cycle. All mice were provided with a standard chow diet (comprising 20.6% proteins, 12% fats, and 67.4% carbohydrates) from Jiangsu Synergetic Pharmaceutical Bioengineering Co., Ltd. Eight-week-old mice weighing 20–22 g were used in this study. Random allocation of groups was conducted using a computer-based random order generator. The investigators performed outcome evaluations while being blinded to the group allocations. Exclusion criteria were established based on the well-being of the animals at the beginning of the study. The sample size was determined based on the experience gained from previous studies involving diabetic animals and KO mice in the laboratory. Littermate control mice were used for all in vivo experiments, and the number of mice used for each experiment is specified in the figure legends. The mice were sacrificed at the end of the experiment by inhaling isoflurane, and tissues were collected for further examination.

We used male C57BL/6J TST KO and WT mice, procured from GemPharmatech Co., Ltd. (C57BL/6JGpt-Tst^{em1Cd1782}/Gpt, Strain No. T044159). We employed the CRISPR/Cas9 technique to delete a 299 bp sequence in exon 2 of the TST gene. Gene targeting verification was achieved by executing PCR on tail DNA. The mouse genotype did not cause visible changes in initial weight, health, or immune status.

For the diabetic mouse model, we administered an intraperitoneal injection of streptozotocin (STZ, Sigma-Aldrich) in 50 mmol/l sodium citrate buffer at 50 mg/kg for 5 consecutive days to 8-week-old fasted male mice, whereas the non-diabetic cohorts were injected with an equal volume of citrate buffer. Approximately 2 weeks post-STZ injection, we considered diabetic groups with blood glucose levels exceeding 16.7 mmol/l as diabetic and incorporated them into the study. Only male mice were used to make the diabetic mouse model in this study as male mice develop more severe diabetic kidney injury. Upon successful diabetes induction, the mice received daily oral administration of 100 μl phosphate-buffered saline (PBS) or STS (0.4 g/kg body weight). The adeno-associated viruses (AAV9) were procured from GeneChem Company, Shanghai, China. Mice were randomized to administered with either 100 μl AAV9-TST or AAV9-Control, each at a concentration of 1×10^{11} VG/ml through the tail vein. We established the diabetic model 2 weeks post-AAV injection, and subsequently the diabetic mouse models were harvested for analysis 12 weeks post-STZ injection.

For the fibrosis model, we randomly allocated 8-week-old male mice to undergo either sham surgery or UUO. The UUO group of mice after anesthetized had their left side of the abdomen shaved, followed by a vertical scalpel incision and skin retraction. To show the kidney, a second incision was performed into the peritoneum. Using 4-0 surgical silk, the left ureter was twice tied off 15 mm below the renal pelvis. The ureter was then severed in the space created by the two ligatures. After that, the ligated kidney was carefully moved back into its proper anatomical position, and fluid loss was restored with sterile saline. In a similar fashion, but without ureteral ligation, the sham operation was carried out. We collected left kidneys for analysis 7 days post-operation.

Blood and urine biochemical analysis

Biochemical analyses of serum parameters, including creatinine (Scr), blood urea nitrogen, glucose, total cholesterol, triacylglycerol, high-density lipoprotein cholesterol, and low-density lipoprotein cholesterol levels, were conducted using an automatic biochemistry analyzer (Biobase, China). To assess the biosafety of STS, serum levels of alanine aminotransferase (ALT)

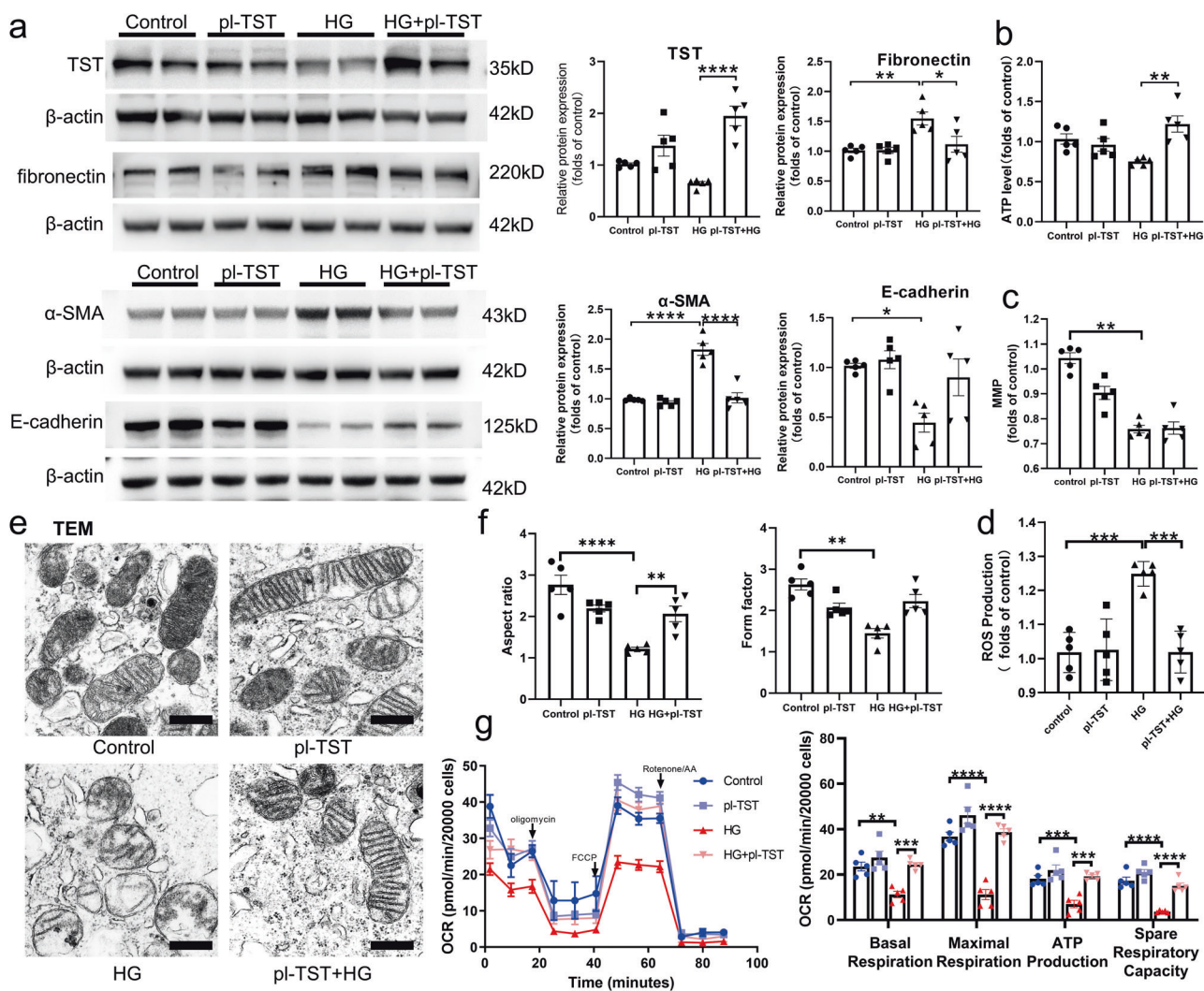


Fig. 4 TST overexpression ameliorated the injury of renal tubular epithelial cells caused by high glucose. **a** Representative western blot images and summarized data shown with the relative protein levels of TST, fibronectin, α -SMA, and E-cadherin in NG or HG-stimulated HK-2 cells transfected with plasmid-blank or plasmid-TST ($n = 5$). **b–d** Measurements of ATP levels, ROS production, and MMP changes in NG or HG-stimulated HK-2 cells transfected with either blank plasmid or TST plasmid ($n = 5$). **e, f** Representative photomicrographs and quantifications of mitochondrial morphological changes in HK-2 cells via TEM analysis ($n = 5$) (Original magnification $\times 15,000$, Scale bars, 500 nm). **g** Oxygen consumption rate (OCR) in HK-2 cells treated with oligomycin (1 $\mu\text{mol/l}$), carbonyl cyanide 4-(trifluoromethoxy)-phenylhydrazone (FCCP, 1 $\mu\text{mol/l}$), and rotenone plus antimycin A (rotenone/AA, 0.5 $\mu\text{mol/l}$), measured using XFe96 extracellular flux analyzer ($n = 5$ for each group). Assessments of basal or maximal respiration, ATP production, and spare respiratory capacity were performed in NG or HG-stimulated HK-2 cells transfected with either blank plasmid or TST plasmid. Data are expressed as mean \pm SEM. * $P < 0.05$, ** $P < 0.01$, *** $P < 0.001$, **** $P < 0.0001$. One-way ANOVA (all multiple comparisons except for form factor in (f)) or Kruskal–Wallis test (form factor in (f)).

and aspartate aminotransferase (AST) were also measured utilizing the same analyzer. For urine biochemical analysis, mice were fasted and individually placed in metabolic cages for urine collection over a period of 6 h. Urinary albumin and creatinine levels in mice were evaluated employing mouse microalbuminuria enzyme-linked immunosorbent assay (ELISA) kit (Elabscience, China) and creatinine (urinary) colorimetric assay kit (Jiancheng, China), respectively, in adherence to the manufacturer's protocols. Urinary levels of Kim-1 were quantified using an ELISA kit (Elabscience, China).

Human sample collection

This research project was conducted according to the Declaration of Helsinki and good clinical practice. The study received approval from the Biomedical Ethics Committee of Zhong Da Hospital, Southeast University (Approval Number: 2019ZDSYL057-P01), and informed consent was obtained from all participants. All methods were carried out in accordance with relevant guidelines and regulations.

Human tissue samples were collected from patients diagnosed with DKD at the Zhong Da Hospital, Southeast University, with verification via renal

biopsy. For comparison, healthy kidney tissues were obtained from nephrectomy patients diagnosed with renal cell carcinoma. Detailed clinical characteristics of these patients are presented in Supplementary Tables 1 and 2.

Immunohistochemical staining

Paraffin-embedded kidney tissue sections, with a thickness of 3 μm , were prepared for IHC staining of α -SMA, E-cadherin, fibronectin, and TST. After dewaxing, heat-induced epitope retrieval was conducted on the kidney sections, which were then blocked using an endogenous peroxidase-blocking solution. Subsequently, primary antibodies (details in Supplementary Table 6) were applied and left to incubate overnight at 4 $^{\circ}\text{C}$. After three washes with PBS, sections were treated with super horseradish peroxidase (HRP) Mouse/Rabbit IHC Kit (MXB Biotechnologies, China), as per the manufacturer's instructions. Peroxidase conjugates were visualized using a Diaminobenzidine (DAB) kit (MXB Biotechnologies, China) and counterstained with hematoxylin. Photomicrographs were captured using an Olympus optical microscope, with analysis conducted using Image J software.

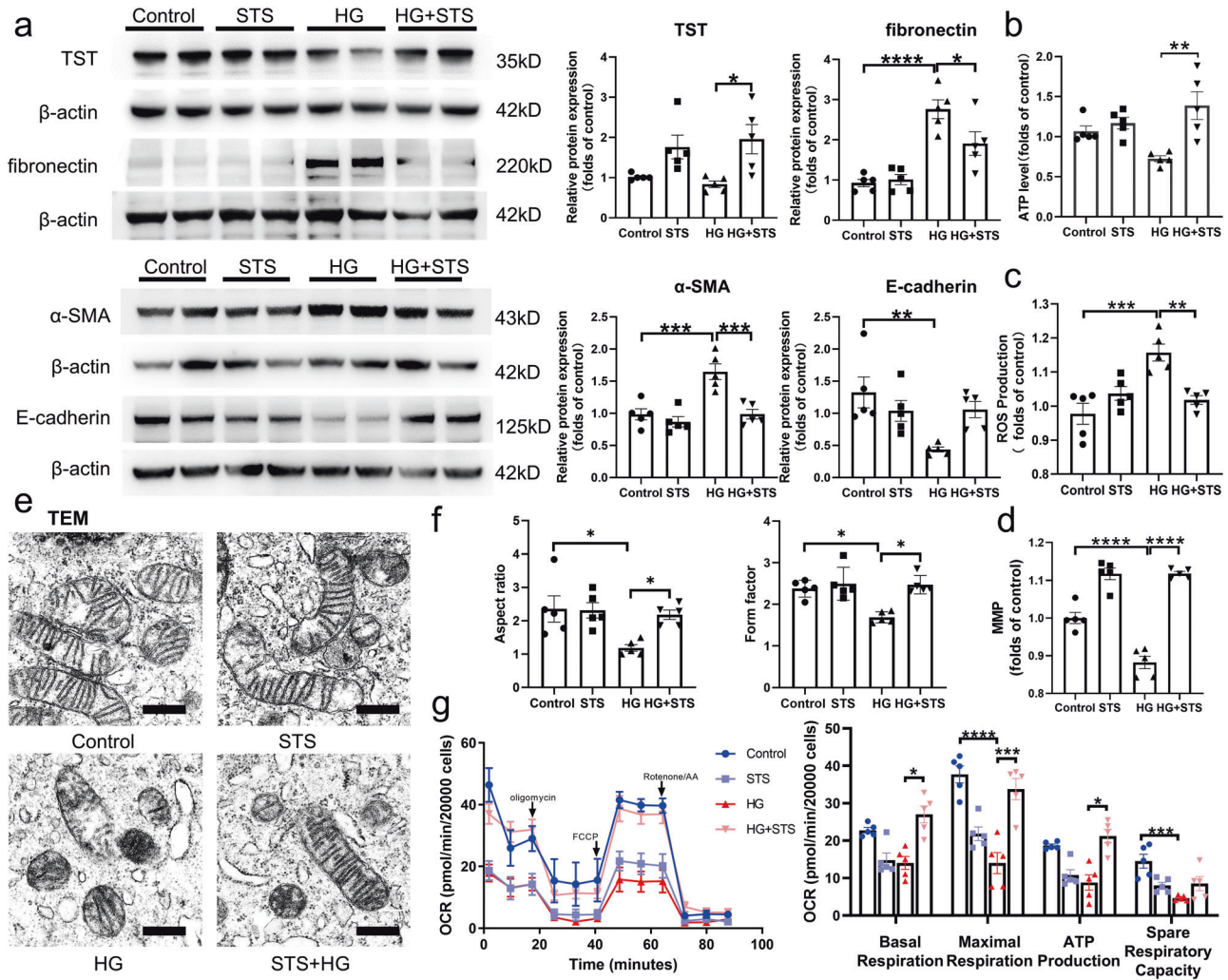


Fig. 5 STS treatment alleviated HG-induced tubular epithelial cell dysfunction and mitochondrial damage. **a** Representative western blot images and summarized data showing the relative protein levels of TST, fibronectin, α -SMA, and E-cadherin in NG or HG-stimulated HK-2 cells with or without STS treatment (10 mmol/l) ($n = 5$). **b–d** Measurements of ATP levels, ROS production, and mitochondrial MMP changes in NG or HG-stimulated HK-2 cells, with or without STS treatment ($n = 5$). **e, f** Representative photomicrographs and quantifications of mitochondrial morphological changes in HK-2 cells via TEM analysis ($n = 5$) (Original magnification $\times 15,000$, Scale bars, 500 nm). **g** OCR examined in HK-2 cells ($n = 5$ for each group). Measurements of basal or maximal respiration, ATP production, and spare respiratory capacity were conducted in NG or HG-stimulated HK-2 cells, with or without STS treatment ($n = 5$). Data are expressed as mean \pm SEM. * $P < 0.05$, ** $P < 0.01$, *** $P < 0.001$, **** $P < 0.0001$. One-way ANOVA (**a, c, d**, aspect ratio in (**f**), maximal respiration and spare respiratory capacity in (**g**)) or Kruskal–Wallis test (**b**, form factor in (**f**), basal respiration and ATP production in (**g**)).

Western blot analysis

Tissue and cell samples were lysed using Radio-Immunoprecipitation Assay lysis buffer (Keygen Biotech, China), supplemented with phosphatase inhibitors (Keygen Biotech, China). Protein concentrations were quantified utilizing a bicinchoninic acid (BCA) protein assay kit (Keygen Biotech, China). Equal concentrations of proteins were then loaded onto sodium dodecyl sulfate-polyacrylamide gels for electrophoresis and subsequently transferred onto an immobilon-P polyvinylidene difluoride (PVDF) membrane (Merk Millipore, USA). Following the blocking with 5% bovine serum albumin (BSA), membranes were incubated overnight at 4 °C with primary antibodies, followed by incubation with HRP-conjugated secondary antibodies for an hour (details in Supplementary Table 6). Protein band intensities were quantified using Image J software. β -actin was used as an internal control and the levels of protein expression normalized to the control group.

Quantitative real-time polymerase chain reaction (qRT-PCR) analysis

Total RNA was isolated from cell samples utilizing the total RNA extraction reagent (Vazyme, China) and subsequently reverse transcribed into cDNA with the aid of the reverse transcription SuperMix (Vazyme, China). The

quantification of mRNA was carried out employing the SYBR qPCR Master Mix (Vazyme, China) and detected via the 7300 Real-Time PCR Detection System (Applied Biosystems, USA). β -actin served as the internal reference. The $2^{-\Delta\Delta CT}$ method was utilized for the quantification of relative gene expression levels. The utilized gene primers are detailed in Supplementary Table 7.

Periodic acid-Schiff (PAS) staining and Masson's trichrome staining

Paraffin-embedded sections of kidney tissue underwent PAS and Masson's trichrome staining to assess renal tubular injury and tubulointerstitial fibrosis, respectively. To determine interstitial fibrosis, a minimum of five images of the kidney cortex (at 400 \times magnification), stained with Masson's trichrome, were randomly selected from each mouse. The presence of blue staining indicated tissue fibrosis. The subsequent quantification of the fibrotic area was executed utilizing Image J software. The tubular injury score was determined by evaluating the severity of tubular dilatation, atrophy, and cell loss as previously reported [39]. Twenty PAS-stained kidney cortex images (at 400 \times magnification) were randomly chosen for per mouse, and the images were evaluated as follows: 0 for no injury, 1 for <25%, 2 for 25%–50%, 3 for 50%–75%, and 4 for >75% tubular injury.

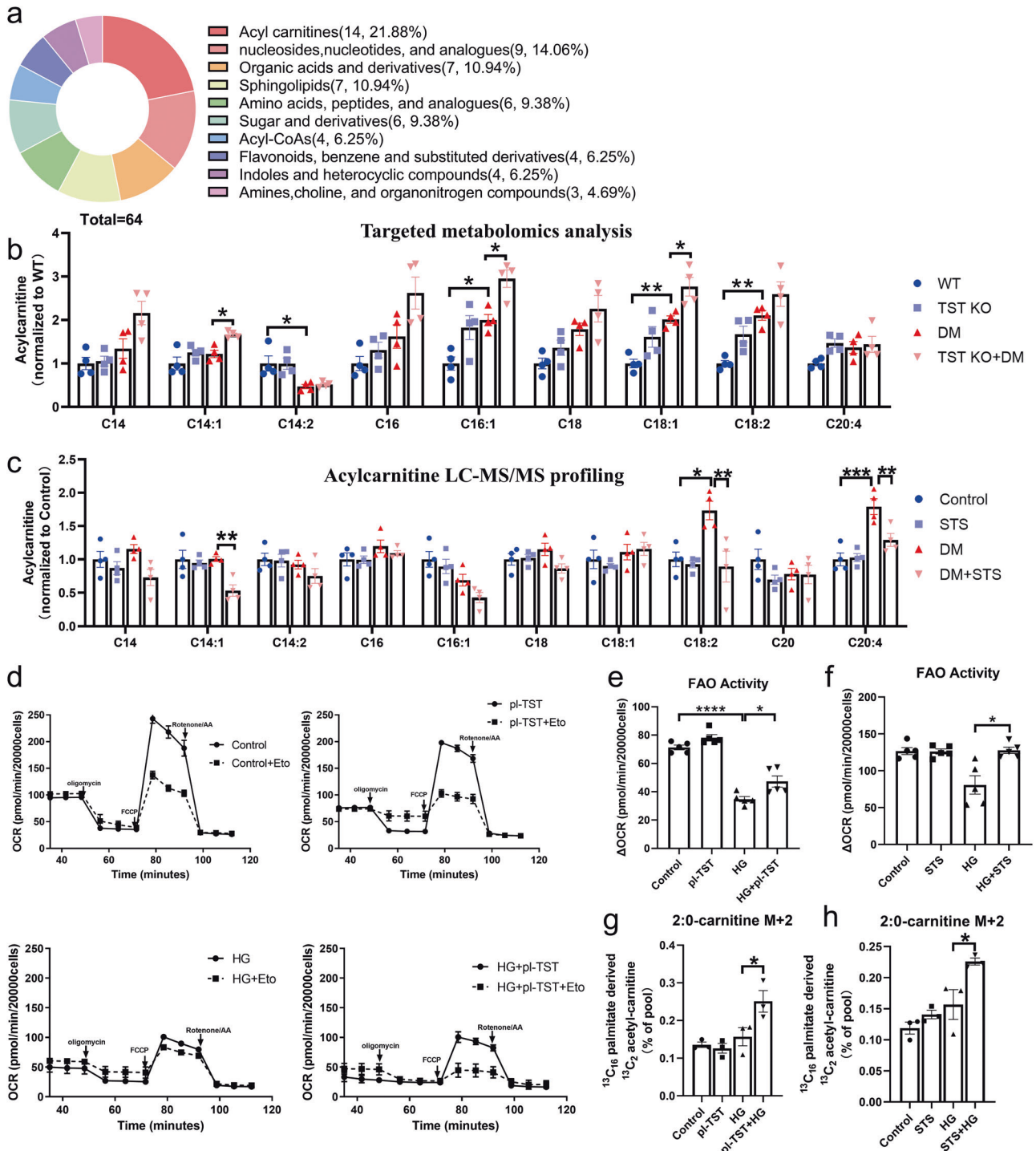


Fig. 6 TST maintained mitochondrial FAO homeostasis in renal tubular epithelial cells in diabetic conditions. **a** Classification of the top 10 most different metabolites from the renal cortex of mice in the WT, TST KO, diabetic WT and TST KO groups (P -value < 0.05 , VIP > 1) ($n = 4$ mice per group). **b** Long-chain acylcarnitine profiles from the kidney cortex of normal or diabetic WT and TST KO mice ($n = 4$) Complete names of acylcarnitines are listed in Supplementary Table 9. **c** Long-chain acylcarnitine profiles from the kidney cortex of diabetic mice with or without STS ($n = 4$). **d**, **e** OCR measured with a Seahorse Bioanalyzer ($n = 5$). The dotted line indicates treatment with $4 \mu\text{mol/l}$ etomoxir (Eto). Mitochondrial FAO activity was calculated as the difference in maximal respiration in PTEC treated with (+Eto) or without etomoxir ($n = 5$). **f** Δ OCR in PTEC treated with or without STS treatment (10 mmol/l) to assess mitochondrial FAO activity ($n = 5$). **g** Levels of $^{13}\text{C}_2$ acetyl-carnitine in NG or HG-stimulated PTEC transfected with plasmid-blank or plasmid-TST ($n = 3$). **h** Levels of $^{13}\text{C}_2$ acetyl-carnitine in NG or HG-stimulated PTEC with or without STS ($n = 3$). Data are expressed as mean \pm SEM. * $P < 0.05$, ** $P < 0.01$, *** $P < 0.001$, **** $P < 0.0001$. One-way ANOVA (**b** except for C18, **c**, **e**, **g**, **h**) or Kruskal–Wallis test (C18 in (**b**), **f**).

Cell culture

The HK-2 tubular epithelial cell line and HEK-293T cell line were obtained from the American Type Cell Culture (ATCC). STR profiling was

used to identify each cell line, and no mycoplasma contamination was found.

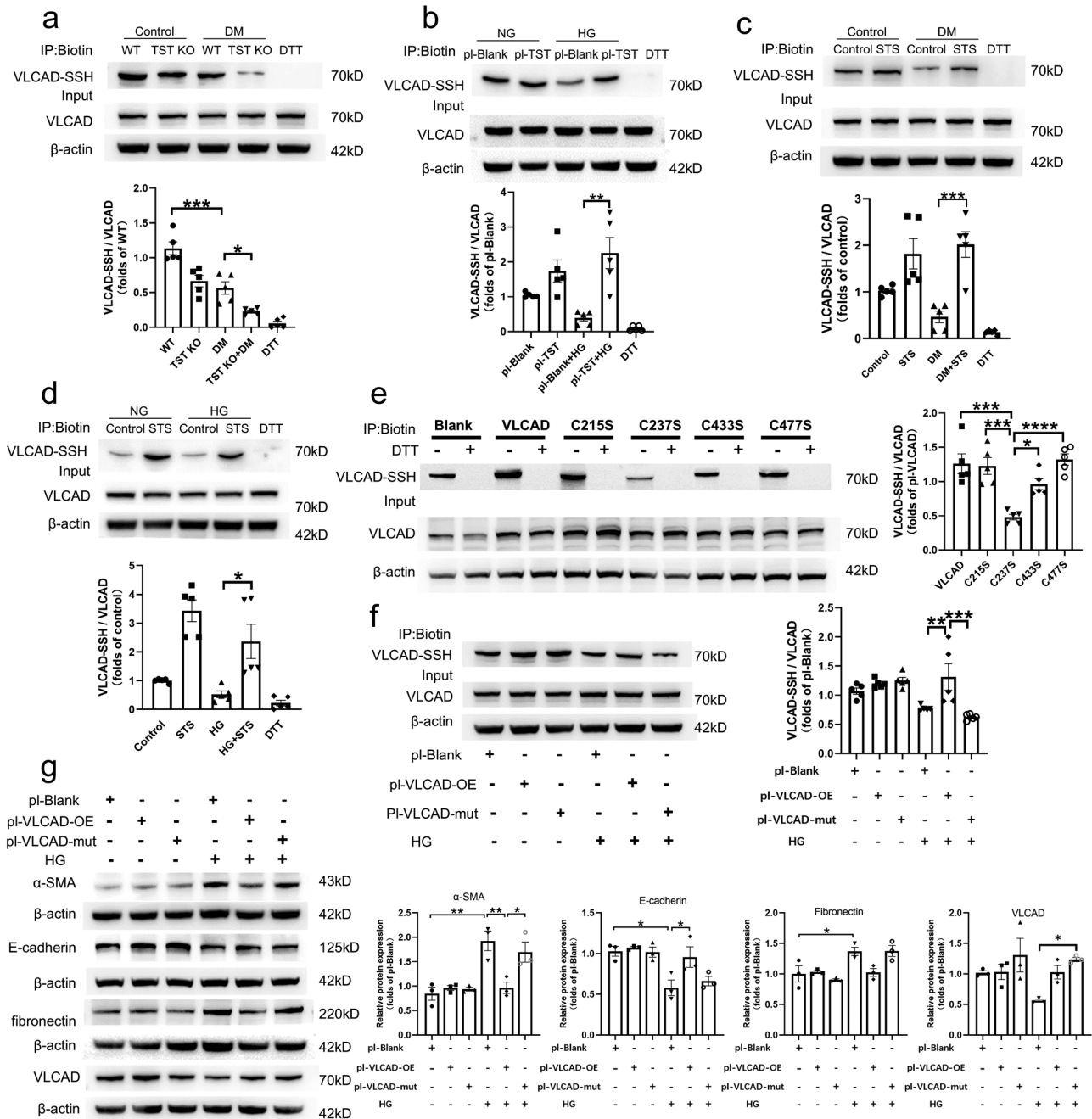


Fig. 7 TST promoted S-sulfhydration of VLCAD. **a** S-sulfhydrated VLCAD (VLCAD-SSH) obtained from the kidney cortex of WT or TST KO mice with or without diabetes, as per the biotin–thiol labeling assay ($n=5$). Specificity was confirmed via signal quenching using DTT. **b** S-sulfhydrated VLCAD observed in NG or HG-stimulated HK-2 cells following transfection with blank plasmid or TST plasmid ($n=5$). **c** S-sulfhydrated VLCAD in the kidney cortex of non-diabetic or diabetic mice, with and without STS treatment ($n=5$). **d** S-sulfhydrated VLCAD in NG or HG-stimulated HK-2 cells, with and without STS treatment (10 mmol/l) ($n=5$). **e** S-sulfhydration of VLCAD in HEK-293T cells expressing either wild-type VLCAD or cysteine mutants ($n=5$). **f** S-sulfhydration of VLCAD in HK-2 cells transfected with either an empty plasmid (pi-Blank), wild-type VLCAD plasmid (pi-VLCAD-OE), or the cysteine mutant C237S plasmid (pi-VLCAD-mut), with or without HG treatment ($n=5$). **g** Representative western blot images and quantified data depicting relative protein levels of VLCAD, fibronectin, α -SMA, and E-cadherin in HK-2 cells transfected with either an empty plasmid (pi-Blank), wild-type VLCAD plasmid (pi-VLCAD-OE) or the cysteine mutant C237S plasmid (pi-VLCAD-mut), with or without HG treatment ($n=3$). Data are expressed as mean \pm SEM. * $P < 0.05$, ** $P < 0.01$, *** $P < 0.001$, **** $P < 0.0001$. One-way ANOVA (all multiple comparisons except for (d)) or Kruskal–Wallis test (d).

HK-2 cells were propagated in Dulbecco's Modified Eagle Medium/Nutrient Mixture F-12 (DMEM/F-12) medium (Wisent Corporation, China), supplemented with 10% fetal bovine serum (FBS) and 1% penicillin/streptomycin, under atmospheric conditions of 95% air and 5% CO_2 . Subsequent to a 6-h nutrient deprivation phase in DMEM/F-12 medium containing 1% penicillin/streptomycin, the HK-2 cells were exposed to distinct treatments, as specified in figure legends. The study

employed a plasmid (Sangon Biotech, China) to induce protein over-expression, thus exploring the mechanism underlying tubulointerstitial injury. Lipofectamine TM 2000 reagent (Invitrogen, USA) was utilized according to the manufacturer's instructions.

HEK-293T cells were cultured in DMEM-HG medium (Wisent Corporation, China), fortified with 10% FBS and 1% penicillin/streptomycin, within an atmosphere comprising 95% air and 5% CO_2 . The HEK-293T cells, post a

6-h fasting period in DMEM-HG media with 1% penicillin/streptomycin, were transfected using a combination of Lipofectamine TM 2000 reagent and various plasmids. The culture medium was replenished following a 6-h transfection period. The plasmid pcDNA3.1-VLCAD and its mutation was purchased from (Sangon Biotech, China). Successful single-site mutation of Cys215, Cys237, Cys433, or Cys477 to serine was confirmed by DNA sequencing.

PTEC were procured from the renal cortex of 3-week-old mice. The isolated cortical tissue was transferred to a Hank's balanced salt solution, meticulously dissected into roughly 1 mm³ fragments, and passed through a series of 70 µm mesh screens. The tissue fragments were subjected to enzymatic digestion with 1 mg/ml type I collagenase (Biosharp, China) at 37 °C for a duration of 25 min. The resulting cell suspension, obtained after passage through a 40 µm mesh, was propagated in DMEM/F-12 medium supplemented with 10% FBS, 1% penicillin/streptomycin, 1% insulin-transferrin-selenium (Gibco), 10 ng/ml epidermal growth factor (Novoprotein, China), and 50 nmol/l hydrocortisone (Selleck). After 48 h of PTEC culture, the medium was replaced. The PTEC were mainly used before the F2 generation. AQP-1 fluorescence was used to determine the purity of the PTEC. Over 80% of all cells express AQP-1 fluorescence, making them usable.

Cell viability and cytotoxicity assessment

The biosafety of STS was evaluated through cell viability and cytotoxicity tests. This was conducted using a cell counting kit-8 (CCK8, Beyotime, China) and a lactate dehydrogenase (LDH) cytotoxicity colorimetric assay (Elabscience, China). The HK-2 cells underwent these tests subsequent to treatment with STS.

Seahorse metabolic assay

An examination of mitochondrial respiration and mitochondrial FAO functionality in cultured cells was conducted utilizing a Seahorse flux analyzer (Agilent Technologies), in adherence to the manufacturer's guidelines. In summary, XF96 cell culture microplates were utilized to culture 2×10^4 cells/well in Agilent Technologies' growth medium. Before the assay, the cells received a thorough rinse with assay medium. For the FAO assay, Eto (4 µmol/l, Selleck) was applied to select wells. The culture then sequentially received oligomycin (1 µmol/l), FCCP (1 µmol/l), and rotenone/antimycin A (0.5 µmol/l). This allowed the assessment of the OCR. As previously described, the assessment of mitochondrial FAO was achieved through the calculation of the difference in maximal respiration levels between cells that underwent treatment with Eto (denoted as "+Eto") and those that did not [11].

Detection of reactive oxygen species (ROS) and mitochondrial membrane potential

Cells, post-digestion, were incubated with either mitosox (4 µmol/l, Invitrogen) or tetramethylrhodamine ethyl ester (1×, Beyotime, China). This process took place in a cell incubator that maintained a 5% CO₂ and 95% air atmosphere at 37 °C away from light, for a duration of 20 min. Following this, cells were rinsed and an equal concentration of cell suspension was placed into a light-proof, black 96-well plate with a transparent bottom. The fluorescence intensity was then gauged using a Varioskan LUX Multimode Microplate Reader (Thermo Scientific).

Adenosine triphosphate (ATP) measurement

The ATP concentration present in the kidneys and cells was ascertained through the ATP colorimetric assay kit (Beyotime, China). Following this, samples were mixed with the ATP probe, converter, and developer. The relative light unit value was determined via chemiluminescence. Finally, the ATP concentration in each sample was calculated in accordance with the luminescence signal and normalized by the protein concentration.

Transmission electron microscopy

Sample tissues and cells were fixed using 2.5% glutaraldehyde at a temperature of 4 °C. The procedure for preparing and analyzing TEM samples was conducted by Wuhan Pinuofei Biological Technology Co., Ltd. Six fields with at least five mitochondria each were randomly selected from TEM images of the renal tubular cells in vivo or HK-2 cells in vitro. The software utilized for analyzing TEM images was Image J. The aspect ratio was determined as the ratio of the major to minor mitochondrial axes. The form factor was defined as the square of the perimeter divided by the

product of 4π and the surface area. The aspect ratio reflects the shape of the mitochondria and the form factor reflects the branching and morphological complexity of mitochondria [40].

S-sulfhydration biotin–thiol labeling assay

S-sulfhydration biotin–thiol labeling assay was performed as previously described [41]. Cells or kidney tissue samples were homogenized using HEN buffer comprising 250 mmol/l HEPES–NaOH (pH 7.7), 1 mmol/l EDTA, 0.1 mmol/l neocuproine, and supplemented with 150 µmol/l deferoxamine, 1% Nonidet-P4, and a cocktail of protease/phosphatase inhibitors. The obtained lysates were combined with HEN buffer fortified with 2.5% SDS and 20 mmol/l methyl methanethiosulfonate (MMTS, Sigma-Aldrich), serving to block free thiols. Excess MMTS was eliminated via pre-cooled acetone. Post-centrifugation, the pellets were resuspended in HEN buffer, which included 1% SDS and 4 mmol/l biotin-HPDP (Sangon Biotech, China). Following a 3-h incubation period at 25 °C, proteins were extracted using acetone. Ultimately, the proteins were dissolved in a solution buffer and purified with streptavidin resin (Sangon Biotech, China). Detection of S-sulfhydrated proteins was performed through SDS–PAGE and western blotting. Each test incorporated a negative control, generated by the inclusion of 1 mmol/l dithiothreitol (DTT) during the biotin cross-linking phase.

Targeted metabolomics analysis

Renal cortex tissues were subjected to targeted metabolomics examination, which was performed by BIOPROFILES (Shanghai, China). BIOPROFILES employed a standardized procedure to prepare the renal samples for analysis by liquid chromatography–tandem mass spectrometry [42]. Statistical analysis was applied to identify metabolites demonstrating differential levels, predicated on *p* values <0.05 and Variable Importance for the Projection (VIP) score exceeding 1.

Acylcarnitine LC–MS/MS profiling

The acylcarnitine profiling was conducted by BIOMS (Beijing, China), utilizing an Acquity ultra-performance liquid chromatography system in combination with a XEVO TQ XS mass spectrometer supplied by Waters Corporation (MA, USA). Data procured from the mass spectrometry were processed employing Target Lynx software from Waters Corporation.

Stable isotope tracing experiment

PTECs after treatment incubated with 50 µmol/l uniformly labeled ¹³C₁₆ palmitate (MedChemExpress) and 100 µmol/l L-carnitine (Selleck) for 12 h. Cells were then collected, counted, washed three times in PBS, and frozen at –80 °C until ultra-performance liquid chromatography analysis. Analysis of acylcarnitines was carried out at LipidALL Technologies as previously described [43].

Statistical analysis

All experimental data represent a minimum of three independent experiments and are expressed as the mean ± standard error of the mean (SEM) using GraphPad Prism 8. Sample sizes are stated in the figure legends and no data were omitted. Statistical significance between the two groups was determined using a two-tailed Student's *t*-test for normally distributed data. For comparisons involving more than two groups, one-way analysis of variance (one-way ANOVA) was used followed by Tukey's multiple comparisons test for normally distributed datasets and Kruskal–Wallis was used followed by Dunn's multiple comparisons test for nonnormally distributed datasets.

DATA AVAILABILITY

We verify that the authors have provided all pertinent data. We have also submitted complete and uncut western blots as Supplementary Material.

REFERENCES

1. Tang S, Yiu WH. Innate immunity in diabetic kidney disease. *Nat Rev Nephrol.* 2020;16:206–22.
2. Li Y, Hu Q, Li C, Liang K, Xiang Y, Hsiao H, et al. PTEN-induced partial epithelial-mesenchymal transition drives diabetic kidney disease. *J Clin Investig.* 2019;129:1129–51.

3. Forbes JM, Thorburn DR. Mitochondrial dysfunction in diabetic kidney disease. *Nat Rev Nephrol.* 2018;14:291–312.
4. Ziyadeh FN. Mediators of diabetic renal disease: the case for TGF-beta as the major mediator. *J Am Soc Nephrol.* 2004;15:S55–S57.
5. Ruiz-Ortega M, Rayego-Mateos S, Lamas S, Ortiz A, Rodrigues-Diez RR. Targeting the progression of chronic kidney disease. *Nat Rev Nephrol.* 2020;16:269–88.
6. Huang S, Susztak K. Epithelial plasticity versus EMT in kidney fibrosis. *Trends Mol Med.* 2016;22:4–6.
7. Miguel V, Tituana J, Herrero JI, Herrero L, Serra D, Cuevas P, et al. Renal tubule cpt1a overexpression protects from kidney fibrosis by restoring mitochondrial homeostasis. *J Clin Investig.* 2021;131:e140695. <https://doi.org/10.1172/JCI140695>.
8. Kang HM, Ahn SH, Choi P, Ko YA, Han SH, Chinga F, et al. Defective fatty acid oxidation in renal tubular epithelial cells has a key role in kidney fibrosis development. *Nat Med.* 2015;21:37–46.
9. Afshinnia F, Rajendiran TM, Soni T, Byun J, Wernisch S, Sas KM, et al. Impaired beta-oxidation and altered complex lipid fatty acid partitioning with advancing CKD. *J Am Soc Nephrol.* 2018;29:295–306.
10. Han SH, Malaga-Dieguez L, Chinga F, Kang HM, Tao J, Reidy K, et al. Deletion of Ikb1 in renal tubular epithelial cells leads to CKD by altering metabolism. *J Am Soc Nephrol.* 2016;27:439–53.
11. Jao TM, Nangaku M, Wu CH, Sugahara M, Saito H, Maekawa H, et al. Atf6a downregulation of PPAR alpha promotes lipotoxicity-induced tubulointerstitial fibrosis. *Kidney Int.* 2019;95:577–89.
12. Lee SY, Kang JM, Kim DJ, Park SH, Jeong HY, Lee YH, et al. Pgc1a activators mitigate diabetic tubulopathy by improving mitochondrial dynamics and quality control. *J Diabetes Res.* 2017;2017:6483572.
13. Houten SM, Violante S, Ventura FV, Wanders RJ. The biochemistry and physiology of mitochondrial fatty acid beta-oxidation and its genetic disorders. *Annu Rev Physiol.* 2016;78:23–44.
14. Diekman EF, Ferdinandusse S, van der Pol L, Waterham HR, Ruiter JP, IJlst L, et al. Fatty acid oxidation flux predicts the clinical severity of VLCAD deficiency. *Genet Med.* 2015;17:989–94.
15. Doulias PT, Tenopoulou M, Greene JL, Raju K, Ischiropoulos H. Nitric oxide regulates mitochondrial fatty acid metabolism through reversible protein S-nitrosylation. *Sci Signal.* 2013;6:s1.
16. Tcheng M, Roma A, Ahmed N, Smith RW, Jayanth P, Minden MD, et al. Very long chain fatty acid metabolism is required in acute myeloid leukemia. *Blood.* 2021;137:3518–32.
17. Kruithof PD, Lunev S, Aguilar LS, de Assis BF, Al-Dahmani ZM, Joles JA, et al. Unraveling the role of thiosulfate sulfurtransferase in metabolic diseases. *Biochim Biophys Acta Mol Basis Dis.* 2020;1866:165716.
18. Morton NM, Beltram J, Carter RN, Michailidou Z, Gorjanc G, Mcfadden C, et al. Genetic identification of thiosulfate sulfurtransferase as an adipocyte-expressed antidiabetic target in mice selected for leanness. *Nat Med.* 2016;22:771–9.
19. Carter RN, Gibbins M, Barrios-Llerena ME, Wilkie SE, Freddolino PL, Libiad M, et al. The hepatic compensatory response to elevated systemic sulfide promotes diabetes. *Cell Rep.* 2021;37:109958.
20. Filipovic MR, Zivanovic J, Alvarez B, Banerjee R. Chemical biology of H₂S signaling through persulfidation. *Chem Rev.* 2018;118:1253–337.
21. Pagani S, Galante YM. Interaction of rhodanese with mitochondrial NADH dehydrogenase. *Biochim Biophys Acta.* 1983;742:278–84.
22. Li A, Yi B, Han H, Yang S, Hu Z, Zheng L, et al. Vitamin D-VDR (vitamin D receptor) regulates defective autophagy in renal tubular epithelial cell in streptozotocin-induced diabetic mice via the AMPK pathway. *Autophagy.* 2022;18:877–90.
23. Brenner M, Azer SM, Oh KJ, Han CH, Lee J, Mahon SB, et al. Oral glycine and sodium thiosulfate for lethal cyanide ingestion. *J Clin Toxicol.* 2017;7:355. <https://doi.org/10.4172/2167-7972.1000355>.
24. Herman-Edelstein M, Scherzer P, Tobar A, Levi M, Gafter U. Altered renal lipid metabolism and renal lipid accumulation in human diabetic nephropathy. *J Lipid Res.* 2014;55:561–72.
25. Zhang J, Muise ES, Han S, Kutchukian PS, Costet P, Zhu Y, et al. Molecular profiling reveals a common metabolic signature of tissue fibrosis. *Cell Rep Med.* 2020;1:100056.
26. Sas KM, Kayampilly P, Byun J, Nair V, Hinder LM, Hur J, et al. Tissue-specific metabolic reprogramming drives nutrient flux in diabetic complications. *JCI Insight.* 2016;1:e86976.
27. Ibarra-Gonzalez I, Cruz-Bautista I, Bello-Chavolla OY, Vela-Amieva M, Pallares-Mendez R, Ruiz DSYN, et al. Optimization of kidney dysfunction prediction in diabetic kidney disease using targeted metabolomics. *Acta Diabetol.* 2018;55:1151–61.
28. Looker HC, Colombo M, Hess S, Brosnan MJ, Farran B, Dalton RN, et al. Biomarkers of rapid chronic kidney disease progression in type 2 diabetes. *Kidney Int.* 2015;88:888–96.
29. Bergman HM, Lindfors L, Palm F, Kihlberg J, Lanekoff I. Metabolite aberrations in early diabetes detected in rat kidney using mass spectrometry imaging. *Anal Bioanal Chem.* 2019;411:2809–16.
30. Brock PR, Maibach R, Childs M, Rajput K, Roebuck D, Sullivan MJ, et al. Sodium thiosulfate for protection from cisplatin-induced hearing loss. *N Engl J Med.* 2018;378:2376–85.
31. Pasch A, Schaffner T, Huynh-Do U, Frey BM, Frey FJ, Farese S. Sodium thiosulfate prevents vascular calcifications in uremic rats. *Kidney Int.* 2008;74:1444–53.
32. Marutani E, Yamada M, Ida T, Tokuda K, Ikeda K, Kai S, et al. Thiosulfate mediates cytoprotective effects of hydrogen sulfide against neuronal ischemia. *J Am Heart Assoc.* 2015;4:e002125. <https://doi.org/10.1161/JAHA.115.002125>.
33. Paul BD, Snyder SH. H₂S signaling through protein sulfhydration and beyond. *Nat Rev Mol Cell Biol.* 2012;13:499–507.
34. Peleli M, Zampas P, Papapetropoulos A. Hydrogen sulfide and the kidney: physiological roles, contribution to pathophysiology, and therapeutic potential. *Antioxid Redox Signal.* 2022;36:220–43.
35. Yuan Y, Zhu L, Li L, Liu J, Chen Y, Cheng J, et al. S-sulfhydration of SIRT3 by hydrogen sulfide attenuates mitochondrial dysfunction in cisplatin-induced acute kidney injury. *Antioxid Redox Signal.* 2019;31:1302–19.
36. Sun HJ, Xiong SP, Cao X, Cao L, Zhu MY, Wu ZY, et al. Polysulfide-mediated sulfhydration of SIRT1 prevents diabetic nephropathy by suppressing phosphorylation and acetylation of p65 NF-kappaB and STAT3. *Redox Biol.* 2021;38:101813.
37. Mathur A, Sims HF, Gopalakrishnan D, Gibson B, Rinaldo P, Vockley J, et al. Molecular heterogeneity in very-long-chain acyl-CoA dehydrogenase deficiency causing pediatric cardiomyopathy and sudden death. *Circulation.* 1999;99:1337–43.
38. Bithi N, Link C, Henderson YO, Kim S, Yang J, Li L, et al. Dietary restriction transforms the mammalian protein persulfidome in a tissue-specific and cystathionine gamma-lyase-dependent manner. *Nat Commun.* 2021;12:1745.
39. Wu L, Liu C, Chang DY, Zhan R, Zhao M, Man LS, et al. The attenuation of diabetic nephropathy by annexin a1 via regulation of lipid metabolism through the AMPK/PPARalpha/CPT1b pathway. *Diabetes.* 2021;70:2192–203.
40. Picard M, White K, Turnbull DM. Mitochondrial morphology, topology, and membrane interactions in skeletal muscle: a quantitative three-dimensional electron microscopy study. *J Appl Physiol.* 2013;114:161–71.
41. Zhao S, Song T, Gu Y, Zhang Y, Cao S, Miao Q, et al. Hydrogen sulfide alleviates liver injury through the S-sulfhydrated-Kelch-like ECH-associated protein 1/nuclear erythroid 2-related factor 2/low-density lipoprotein receptor-related protein 1 pathway. *Hepatology.* 2021;73:282–302.
42. Liu Y, Zhang H, Fan C, Liu F, Li S, Li J, et al. Potential role of BCL2 in lipid metabolism and synaptic dysfunction of age-related hearing loss. *Neurobiol Dis.* 2023;187:106320.
43. Basu SS, Mesaros C, Gelhaus SL, Blair IA. Stable isotope labeling by essential nutrients in cell culture for preparation of labeled coenzyme A and its thioesters. *Anal Chem.* 2011;83:1363–9.

AUTHOR CONTRIBUTIONS

KLM and JXZ performed the study concept and design; PPC, JXZ, and XQL performed the experiments. The data were analyzed by LL, GHW, QYW; JXZ, KLM, and XZR drafted and revised the manuscript. KLM and XZR have verified the underlying data. All authors had access to the data, reviewed the manuscript, and approved the final version for submission.

FUNDING

This study was supported by the National Natural Science Foundation of China (82170736, 81970629, 82370716), and the Natural Science Foundation of Zhejiang Province (LHDMY23H070002).

COMPETING INTERESTS

The authors declare no competing interests.

ETHICS APPROVAL AND CONSENT TO PARTICIPATE

Animal studies were approved by the Animal Care and Use Committee of Southeast University (Approval No. 20210227025). All human studies were performed with informed patient consent and were approved from the Biomedical Ethics Committee of Zhong Da Hospital, Southeast University (Approval Number: 2019ZDSYLL057-P01). All methods were carried out in accordance with relevant guidelines and regulations.

ADDITIONAL INFORMATION

Supplementary information The online version contains supplementary material available at <https://doi.org/10.1038/s41418-024-01365-8>.

Correspondence and requests for materials should be addressed to Kun Ling Ma.

Reprints and permission information is available at <http://www.nature.com/reprints>

Publisher's note Springer Nature remains neutral with regard to jurisdictional claims in published maps and institutional affiliations.

Springer Nature or its licensor (e.g. a society or other partner) holds exclusive rights to this article under a publishing agreement with the author(s) or other rightsholder(s); author self-archiving of the accepted manuscript version of this article is solely governed by the terms of such publishing agreement and applicable law.